Drought-induced mortality of a Bornean tropical rain forest amplified by climate change

Tomo'omi Kumagai[1,2] and Amilcare Porporato[2]

Received 12 August 2011; revised 17 May 2012; accepted 20 May 2012; published 30 June 2012.

[1] Drought-related tree mortality at a regional scale causes drastic shifts in carbon and water cycling in Southeast Asian tropical rain forests, where severe droughts are projected to occur more frequently, especially under El Niño conditions. We examine how the mortality of a Bornean tropical rain forest is altered by projected shifts in rainfall, using field measurements, global climate model (GCM) simulation outputs, and an index developed for drought-induced tree mortality (Tree Death Index η) associated with a stochastic ecohydrological model. All model parameters have clear physical meanings and were obtained by field observations. Rainfall statistics as primary model forcing terms are constructed from long-term rainfall records for the late 20th century, and 14 GCM rainfall projections for the late 21st century. These statistics indicate that there were sporadic severe droughts corresponding with El Niño events, generally occurring in January–March, and that seasonality in rainfall will become more pronounced, e.g., dry (January–March) seasons becoming drier and wet (October–December) seasons becoming wetter. The computed η well reflects high tree mortality under severe drought during the 1997–1998 El Niño event. For the present, model results demonstrate high and low probabilities of mortality in January–March and October–December, respectively, and they predict that the difference in such probabilities will increase in the future. Such high probability of mortality in the dry season is still significantly high, even considering the beneficial effect of increased soil water storage in the wet season (which is projected to increase in the late 21st century).

Citation: Kumagai, T., and A. Porporato (2012), Drought-induced mortality of a Bornean tropical rain forest amplified by climate change, *J. Geophys. Res.*, *117*, G02032, doi:10.1029/2011JG001835.

1. Introduction

[2] Tropical forests receive high radiative energy, playing a significant role in the global carbon budget [*Melillo et al.*, 1993; *Field et al.*, 1998; *Malhi and Grace*, 2000; *Grace et al.*, 2001], and are a major source of global hydrologic fluxes, profoundly influencing both global and regional climates [*Lean and Warrilow*, 1989; *Nobre et al.*, 1991; *Kanae et al.*, 2001; *Avissar and Werth*, 2005]. Since tropical rain forests exist where ecosystem water resources are greatest, perturbations in rainfall regime could significantly change ecological patterns and processes [e.g., *Malhi et al.*, 2009; *Phillips et al.*, 2009], in turn potentially affecting feedbacks to the atmosphere [e.g., *Meir et al.*, 2006; *Bonan*, 2008].

[3] Although tropical forests in Southeast Asia represent only about 11% of the world's tropical forests in terms of area [*World Resources Institute*, 2007], they have the highest relative deforestation rate in tropical areas [*Houghton and Hackler*, 1999; *Laurance*, 1999; *Malhi and Grace*, 2000; *Canadell et al.*, 2007]. Therefore, the impact of these forests is of great concern for global and regional climate and hydrologic cycling [*Kanae et al.*, 2001; *Malhi and Wright*, 2004; *Mabuchi et al.*, 2005; *Werth and Avissar*, 2005]. An analysis of climatic trends in global tropical rain forest regions over the period 1960–1998 showed that rainfall has declined more significantly in Southeast Asia than in Amazonia, and that the El Niño Southern Oscillation (ENSO) may be the primary driver of drought in Southeast Asia [*Malhi and Wright*, 2004] (the Indian Ocean Dipole (IOD) may also cause drought in this region). As summarized by the *Intergovernmental Panel on Climate Change* [2007], the projected growth of atmospheric greenhouse gases in this century will significantly impact global and regional temperatures, with concomitant modifications to precipitation patterns. Global climate models (GCM) have shown more frequent El Niño-like conditions from human-induced greenhouse warming [*Timmermann et al.*, 1999], linked to mechanisms of tropical droughts [*Neelin et al.*, 2003]. Thus, an understanding of how tropical rain forest ecosystems in

[1]Hydrospheric Atmospheric Research Center, Nagoya University, Nagoya, Japan.
[2]Department of Civil and Environmental Engineering, Duke University, Durham, North Carolina, USA.

Corresponding author: T. Kumagai, Hydrospheric Atmospheric Research Center, Nagoya University, Chikusa-ku, Nagoya 464-8601, Japan. (tomoomikumagai@gmail.com)

0148-0227/12/2011JG001835

Southeast Asia respond to climate change and El Niño-induced drought will significantly impact our ability to predict Earth system processes under climate change.

[4] Tree mortality and die-offs at the landscape/regional scale are among the most important forest responses to severe drought. Such regional scale mortality may cause rapid and large-scale shifts in ecosystem structure and function, resulting in drastic changes in carbon, water and energy exchange between biosphere and atmosphere [e.g., *Bonan*, 2008]. Drought-induced tree mortality can be amplified by climate change directly through increasing temperature and drought, and indirectly through favoring demographics of insects and pathogens [*Breshears et al.*, 2005, 2009; *McDowell et al.*, 2008; *Adams et al.*, 2010; *Allen et al.*, 2010]. Furthermore, such profound effects of tree mortality on Earth system processes could generate positive feedbacks that exacerbate climate change [*Betts et al.*, 2004; *Malhi et al.*, 2009; *Adams et al.*, 2010; *Allen et al.*, 2010]. Thus, physiological mechanisms underlying tree survival and mortality during drought should be considered in the context of climate change, but such mechanisms remain poorly understood despite numerous scientific investigations [*McDowell et al.*, 2008; *Allen et al.*, 2010].

[5] Categorizing plants by "isohydric" and "anisohydric" regulation of water status helps link basic drought physiological traits to climate-induced mortality and die-off [e.g., *McDowell et al.*, 2008; *Breshears et al.*, 2009; *Kumagai and Porporato*, 2012]. Isohydric plants regulate transpiration by stomatal closure to maintain constant midday leaf water potential, thus avoiding drought-induced hydraulic failure. However, stomatal closure over longer droughts causes carbon starvation and low production of defensive chemicals against biotic agents, resulting in tree mortality. Further, a rise in temperature and severe drought could accelerate carbon starvation for isohydric plants, because of increased respiration costs [e.g., *Damesin*, 2003; *Metcalfe et al.*, 2010a, 2010b]. In contrast, anisohydric plants have less stomatal sensitivity, and allow midday leaf water potential to decline with soil moisture decrease. Thus, hydraulic failure for these plants occurs at a much more negative water potential than for isohydric species [e.g., *Linton et al.*, 1998; *West et al.*, 2007]. This fact may help anisohydric species to stave off carbon starvation during moderate but long droughts, but it makes them more susceptible to hydraulic failure.

[6] Previous studies and an ongoing throughfall exclusion experiment indicate that the studied tropical rain forest ecosystem tends to have little regulation of forest water use, regardless of sporadically severe soil drying [*Kumagai et al.*, 2004c, 2005; *Kumagai and Porporato*, 2012]. Although it is generally thought that anisohydric behavior is an adaptation to more drought-prone habitats, we showed that anisohydric plants are more favored than isohydric plants under very moist environments where there is little risk of hydraulic failure [*Kumagai and Porporato*, 2012]. Furthermore, there is recent evidence that avoiding the risk of hydraulic failure is the best strategy for water use, in both isohydric and anisohydric species [*Meinzer et al.*, 2009; *McDowell*, 2011]. Thus, here we use a "Tree Death Index," η [*Kumagai and Porporato*, 2012], which focuses on tree death induced only by hydraulic failure assuming anisohydric behavior in the studied forest, and evaluates the impact of climate factors on forest mortality. Nevertheless, in some cases of isohydric plants, one should take into consideration the effect of carbon starvation on tree death [e.g., *Fisher et al.*, 2010].

[7] Our major goal is to clarify how the mortality of a Bornean (Southeast Asia) tropical rain forest will respond to current and projected rainfall patterns. With this goal in mind, we use the Tree Death Index η, which is thought to be the best index for describing tree mortality risk in this region. However, using simply η is insufficient because of its inadequate description of seasonality in rainfall (detailed later). The index is useful for defining actual tree mortality, and for development of a vegetation dynamics model that considers effects of climate-change drought on tree death and survival. Thus, a secondary goal is to show the development, correction and usefulness of η.

[8] The studied rain forest is among the moistest biomes in the world [see *Kumagai et al.*, 2005, Figure 3]. It has been reported that in tropical rain forests of Malaysia and Indonesian Borneo, severe drought associated with the ENSO event of 1997–1998 caused extremely high tree mortality [*Nakagawa et al.*, 2000; *Potts*, 2003; *van Nieuwstadt and Sheil*, 2005; *Allen et al.*, 2010; *Phillips et al.*, 2010]. For the studied Bornean tropical rain forest, we use tree mortality before and after the 1997–1998 El Niño, rainfall records from 1968 to 2001, GCM simulation outputs of current and future rainfall statistics, and η. Based on the anisohydric behavior observed in this forest and the soil–plant–atmosphere continuum (SPAC) concept, η allows use of information from previous detailed field measurements [*Kumagai et al.*, 2004a, 2004b, 2004c, 2005, 2009; *Manfroi et al.*, 2006] and provides model parameters with clear physical meanings. The tree mortality analysis using η is based on stochastic representation of rainfall constructed from long-term rainfall records for the current rainfall scenario, and is linked to GCM simulation outputs for the future rainfall scenario. It thus provides an index of drought-induced mortality, η, for the tropical rain forest, under current climate conditions including sporadic El Niño events, and under future scenarios of global change. We expect that η was larger in the period 1997–1998 and under global change conditions. Furthermore, global change is projected to affect seasonality in rainfall, and thus seasonality in η. In this study, we will confirm these hypotheses and explain the occurrence probability of η under the hypotheses.

2. Theory

[9] Soil moisture dynamics is a key control on hydrologic fluxes through the SPAC, and is fundamental for describing ecosystem processes such as plant water stress [*Porporato et al.*, 2001, 2004; *Rodríguez-Iturbe and Porporato*, 2004]. Accounting only for changes in mean responses to climatic variability is inadequate for realistic investigation of climate change impacts on ecosystems. One must also account for the stochastic component of hydrologic forcing and possible alterations in frequency and amount of rainfall events, which in turn impact soil moisture dynamics and temporal characteristics (i.e., intensity, duration, and frequency) of periods of plant water stress, plant productivity and mortality [*Porporato et al.*, 2001, 2004]. Such probabilistic descriptions of ecosystem process dynamics are useful for assessing the impact of climatic fluctuations, such as severe drought

brought on by current ENSO cycles and global change, whose characterization is inherently affected by uncertainty.

[10] In this study, we use a simple SPAC model linked to probabilistic descriptions of soil moisture and plant water stress [*Porporato et al.*, 2001]. We also develop the index η, representing anisohydric plant mortality (i.e., neglecting carbon starvation-type mortality) produced by climate change-type drought [*Kumagai and Porporato*, 2012]. A review and description of the modeling scheme is presented below for completeness.

2.1. Stochastic Soil Moisture Dynamics Model

[11] The stochastic soil moisture model of this study was originally proposed by *Rodríguez-Iturbe et al.* [1999], and improved by *Laio et al.* [2001]. Under conditions where lateral movement can be neglected, the daily, vertically integrated soil moisture balance equation is given by

$$nZ_r \frac{ds(t)}{dt} = \varphi[s(t), t] - \chi[s(t)], \tag{1}$$

where n is soil porosity; Z_r is rooting depth (mm); s is the degree of saturation between 0 and 1; t is time (day); φ is rate of infiltration into the rooting zone (mm day^{-1}), which is represented by the rainfall rate minus the rate of rainfall loss through canopy interception and rate of infiltration-excess; and χ is the rate of water loss from the soil (mm day^{-1}), i.e., the evapotranspiration rate $E(s, t)$ (mm day^{-1}) plus the leakage $L(s)$ (mm day^{-1}). The frequency of rainfall events can be assumed to be a stochastic variable expressed as an exponential distribution, with mean time interval between precipitation events $1/\lambda$ (day). The amount of rainfall, when it occurs, is also assumed an independent random variable described by an exponential probability distribution, with mean depth of rainfall events α (mm). Losses to the atmosphere from canopy interception are represented using a threshold of rainfall depth Δ (mm) that denotes interception capacity determined by forest stand throughfall and stemflow measurements [e.g., *Manfroi et al.*, 2006], below which effectively no water reaches the ground. Saturation overland flow is derived from rainfall excess, which occurs when rainfall depth exceeds water storage capacity in the rooting zone soil layer.

[12] Leakage losses are assumed to occur through gravitational flow. $L(s)$ is assumed to be at its maximum for saturated soil moisture conditions. It can be expressed as the hydraulic conductivity $K(s)$ (mm day^{-1}), i.e., the exponential function of K_{sat}, the saturated hydraulic conductivity (mm day^{-1}), s_{fc}, s at "field capacity," the water content held in the soil after gravity drainage where $K(s)$ is zero, and β, a parameter that can be obtained by fitting the power law unsaturated hydraulic conductivity to field data [*Laio et al.*, 2001].

[13] In this model, it is considered that the main control on evapotranspiration is s, giving

$$E(s,t) = \begin{cases} 0, & \text{for} \quad 0 < s(t) \le s_h \\ E_W \dfrac{s(t) - s_h}{s_W - s_h}, & \text{for} \quad s_h < s(t) \le s_W \\ E_W + (E_{\max} - E_W)\dfrac{s(t) - s_W}{s^* - s_W}, & \text{for} \quad s_W < s(t) \le s^* \\ E_{\max}, & \text{for} \quad s^* < s(t) \le 1 \end{cases}, \tag{2}$$

where E_W and $E_{\max}$ are soil evaporation and the maximum evapotranspiration (mm day^{-1}), respectively; and s_h, s_W and s^* are s at "hygroscopic point," "plant wilting point," and "plant stress point," respectively. The primary forcing variable for evapotranspiration in the tropics is net available energy [*Kumagai et al.*, 2005]. Thus, we use a modified expression of *Priestley and Taylor* [1972] to compute E_W and $E_{\max}$, given by

$$E_i = \kappa \alpha_{PT\_i} \frac{\delta}{L_v \rho_w (\delta + \varepsilon)} R_n, \tag{3}$$

where i denotes W or max; α_{PT_W} and $\alpha_{PT\_\max}$ are the Priestley–Taylor coefficients (α_{PT}) for E_W and $E_{\max}$, respectively; κ is a unit conversion factor (mm day^{-1} (m s^{-1})$^{-1}$); δ is the rate of change of saturation water vapor pressure with temperature (Pa K^{-1}); L_v is the latent heat of vaporization of water (J kg^{-1}); ρ_w is the density of water (1000 kg m^{-3}); ε is the psychrometric constant (66.5 Pa K^{-1}); and R_n is net radiation above the canopy (W m^{-2}). A major uncertainty in equation (3) is α_{PT}, which for forested ecosystems is usually less than its typical 1.26 value because of additional boundary layer, leaf, xylem, and root resistances. Measured daily evapotranspiration and daily averaged R_n are used to obtain daily α_{PT}, and then we derive a relationship between s and daily α_{PT}. α_{PT_W} and $\alpha_{PT\_\max}$ are parameterized by fitting equations (2) and (3) to the relationship. For the stochastic model computations, all thermodynamic variables in equation (3) are assumed constant, and R_n is obtained by averaging seasonally observed values, to maintain analytical tractability.

[14] Owing to the stochastic rainfall forcing in equation (1), its solution can be represented only in a probabilistic manner. In this framework, the steady state probability density function (PDF) of s, $pdf(s)$, can be derived from the master equation of the process [see *Rodríguez-Iturbe and Porporato*, 2004].

2.2. Plant Water Stress Dynamics and Mortality Model

[15] Following *Porporato et al.* [2001], a (static) plant water stress ζ can be defined as zero when soil moisture is greater than the level of incipient stomatal closure, s^*, and as a maximum of one when soil moisture reaches the level of complete stomatal closure, s_W. A nonlinear curve between s^* and s_W is

$$\zeta(t) = \begin{cases} 1, & \text{for} \quad s(t) \le s_W \\ \left[\dfrac{s^* - s(t)}{s^* - s_W}\right]^q, & \text{for} \quad s_W < s(t) \le s^* \\ 0, & \text{for} \quad s^* < s(t) \end{cases}, \tag{4}$$

where q is a measure of nonlinearity of the effect of soil moisture deficit on plant conditions, varying with plant species. Plants with a higher q value, i.e., stronger nonlinearity, can have lower ζ with decreasing s, but abruptly increase ζ in the immediate vicinity of s_W. This means that such plants can allow their leaf water potential to approach the xylem cavitation threshold without suffering from water stress [*Porporato et al.*, 2001].

[16] The probabilistic structure of ζ can be derived from $pdf(s)$ by substituting equation (4) for s. The PDF of ζ, $f_Z(\zeta)$, has an atom of probability at $\zeta = 0$, $F_Z(0) = 1 - P(s^*)$, and

one at $\zeta = 1$ equal to $F_Z(1) = P(s_W)$ (where P is the cumulative density function of s). The continuous part of $f_Z(\zeta)$ between zero and one, corresponding to $s_W < s < s^*$, can be written as [*Porporato et al.*, 2001]:

$$f_Z(\zeta) = \frac{C_\zeta}{\xi_W}\left[\left(1-\frac{\xi}{\xi_W}\right)\zeta^{\frac{1}{q}} + \frac{\xi}{\xi_W}\right]^{\lambda'\frac{s^*-s_W}{\xi-\xi_W}-1} \exp\left\{\mu\left[(s^*-s_W)\zeta^{\frac{1}{q}} - s^*\right]\right\}, \tag{5}$$

in which

$$\xi_W = \frac{E_W}{nZ_r},\ \xi = \frac{E_{\max}}{nZ_r},\ \mu = \frac{nZ_r}{\alpha}, \tag{6}$$

where C_ζ is an integration constant that can be found by imposing the condition $F_Z(0) + F_Z(1) + \int_0^1 f_Z(\zeta)d\zeta = 1$.

[17] Mean water stress can be calculated as $\overline{\zeta} = \int_0^1 \zeta f_Z(\zeta)\, d\zeta + F_Z(1)$. However, since the value of $\overline{\zeta}$ also takes into consideration periods of $\zeta = 0$, we thus consider the mean value of water stress (assuming the plant is under stress) as [*Porporato et al.*, 2001]:

$$\overline{\zeta'} = \frac{\overline{\zeta}}{P(s^*)}, \tag{7}$$

where $P(s^*)$ denotes only that part of the PDF corresponding to ζ above 0.

[18] The information on plant conditions given by the mean and the PDF of water stress must be completed by a description of the temporal characteristics of periods of water stress. The length of the periods in which soil moisture is below a threshold is among the important stochastic variables in the treatment of this temporal dimension of water stress. The analytical expression for the mean duration of an excursion below the threshold s_W ($\overline{T_{s_W}}$; day) can be obtained using the crossing analysis as [*Porporato et al.*, 2001]:

$$\overline{T_{s_W}} = \frac{1}{\lambda'} + \frac{1}{\lambda'}[\mu(s_W - s_h)]^{-\lambda'\frac{s_W-s_h}{\xi_W}}\gamma\left[1+\lambda'\frac{s_W-s_h}{\xi_W}, \mu(s_W-s_h)\right] \cdot \exp[\mu(s_W-s_h)], \tag{8}$$

where λ' is the frequency of rainfall events (day^{-1}) given by $\lambda \exp(-\Delta/\alpha)$; and $\gamma[\cdot,\cdot]$ is the lower incomplete Gamma function.

[19] *Porporato et al.* [2001] defined a measure of vegetation water stress by combining $\overline{\zeta'}$ with the mean duration and frequency of water stress during the growing season, calling it "dynamic" water stress or mean total dynamic stress during that season, $\overline{\theta}$. Likewise, to describe plant mortality and survival caused by hydraulic failure under severe drought conditions, we define a "Tree Death Index" η, using equations (7) and (8) as

$$\eta = \begin{cases} \dfrac{\overline{\zeta'}\,\overline{T_{s_W}}}{kT_{seas}} & \text{if } \overline{\zeta'}\,\overline{T_{s_W}} < kT_{seas}, \\ 1 & \text{otherwise}, \end{cases} \tag{9}$$

where k is a parameter representing an index of plant resistance to drought, which can vary with plant species. The mortality of plants with a higher-k value is insensitive to drought conditions described by $\overline{\zeta'}$ and $\overline{T_{s_W}}$. T_{seas} is the number of days in a season (day). Tree mortality described by η is related to permanent damage from drought-induced hydraulic failure. Unlike the $\overline{\theta}$ given by *Porporato et al.*, we use $\overline{T_{s_W}}$ instead of the mean duration of an excursion below s^*. Moreover, we do not take into account the effect of frequency of water stress in equation (9), because permanent damage leading to tree mortality occurs at maximum water stress, and tree mortality is a single event in time.

[20] With seasonal variation in rainfall, i.e., wet and dry seasons, the effect of wet season soil moisture storage on subsequent dry season forest water use becomes crucial in the strategy of vegetation to cope with stochastic water availability [*Kumagai et al.*, 2009]. To account for this effect, we use the mean time $\overline{T}_{s^*}(s_0)$ (day) to reach the threshold of water stress s^*, from an arbitrary soil water content s_0 at the dry season start, as given by *Rodríguez-Iturbe and Porporato* [2004]:

$$\overline{T}_{s^*}(s_0) = \int_{s^*}^{s_0} \frac{\lambda[1-P(u)] - \rho(u)pdf(u)}{[\rho(u)]^2 pdf(u)}\, du, \tag{10}$$

where $\rho(u)$ is the normalized loss function described as $\chi(u)/nZ_r$. To explain the effect of possible water storage at growing season start on plant water stress during the season, *Rodríguez-Iturbe et al.* [2001] extended $\overline{\theta}$, assuming that water stress is zero at that start, until $s(t)$ reaches s^*, when it equals $\overline{\theta}$. Likewise, to describe the dry season η affected by the preceding wet season water storage, using $\overline{T}_{s^*}(s_0)$, we defined a corrected η as

$$\eta' = \frac{T_{seas} - \overline{T}_{s^*}(s_0)}{T_{seas}}\eta \tag{11}$$

Here, we use the steady state η during a season and a specific period (e.g., El Niño event), its interannual variation, and the corrected η to account for the effect of preceding wet season water storage η', in the analysis of plant mortality and survival under drought conditions caused by a historical El Niño event and climate change.

3. Materials and Methods

3.1. Site Description and SPAC Model Parameters

[21] Vegetation–atmosphere exchange and meteorological data, which are well suited for estimating the SPAC model parameters, were obtained for a natural forest in Lambir Hills National Park (LHNP; 4°12′N, 114°02′E, 200 m a.s.l.), 30 km south of the city of Miri in Sarawak, Malaysia. The mean annual temperature in LHNP is around 27°C, with little seasonal variation. The rain forest in LHNP consists of two types of original vegetation common to Borneo, mixed dipterocarp and tropical heath forest. The former contains various genera of the family Dipterocarpaceae, which covers 85% of LHNP. Average canopy height at the study site is about 40 m, but heights of emergent treetops can reach 50 m. The leaf area index (LAI) ranged spatially from 4.8 to 6.8 m^2 m^{-2}, with mean 6.2 m^2 m^{-2}. The monthly amounts of litterfall were similar throughout the year, suggesting small variations in LAI. Soils consist of red-yellow podzolic (Malaysian classification) or Ultisols (United States

Table 1. Model Parameters of Evapotranspiration and Soil Characteristics in Lambir Hills National Park

Parameter	Definition	Value
Z_r (mm)	Rooting depth in equation (1)	1000
n	Soil porosity in equation (1)	0.36
K_{sat} (mm day^{-1})	Saturated hydraulic conductivity	33.4
β	Exponent of soil-water retention curve	6.3
s_h	Soil moisture as degree saturation (s) at hygroscopic point in equation (2)	0.05
s_W	s at plant wilting point, in equations (2) and (4)	0.1
s^*	s at plant stress point, in equations (2) and (4)	0.34
s_{fc}	s at field capacity	0.34
α_{PT_W}	Priestley-Taylor coefficient (α_{PT}) for soil evaporation in equation (3)	0.57
α_{PT_max}	α_{PT} for maximum evapotranspiration in equation (3)	0.82
R_n for Oct-May (W m^{-2})	Net radiation above canopy (R_n) for wet season in equation (3)	128.3
R_n for Apr-Sep (W m^{-2})	R_n for dry season in equation (3)	140.3
q	Nonlinearity of soil moisture deficit effect on plant conditions, in equation (4)	3
Δ (mm)	Interception capacity	1.10

Department of Agriculture Soil Taxonomy), with high sand content (62–72%), accumulation of nutrient content at the surface horizon, low pH (4.0–4.3), and high porosity (54–68%). Oxisols are widely distributed in the African and South American tropics, and are rarely seen in the Southeast Asian tropics. Ultisols, however, which are classified as an argillic soil, prevail in the Southeast Asian tropics, suggesting the representative soil type in this region.

[22] A 4 ha experimental plot gridded into 400 subplots of 10 m × 10 m was established in LHNP. An 80-m-tall (to the gondola base) canopy crane with a 75-m-long rotating jib was constructed at the center of this plot, to provide access to the upper canopy. Some observational floors of the canopy crane were devoted to eddy covariance flux measurements and above-canopy meteorological measurements, such as radiation flux, air temperature and humidity, wind velocity and rainfall. The subplots were used for throughfall and stemflow measurements, in-canopy micrometeorological measurements and soil moisture measurements.

[23] Table 1 gives model parameters for evapotranspiration and soil characteristics, for computing soil moisture dynamics in LHNP. Derivation of these parameters and how computation results were validated are described elsewhere [*Kumagai et al.*, 2009], but a brief description is provided here for completeness.

[24] We used eddy covariance-measured transpiration to derive relationships between s and daily α_{PT} for the present vegetation, according to the procedure in the description of equation (3) (see section 2.1) [*Kumagai et al.*, 2004b]. Given the high LAI at the site (>3), bulk surface conductance (G_s) is strongly related to the behavior of leaf stomatal conductance (g_s), and can be fixed at a value about three times that of g_s, independent of LAI [*Kelliher et al.*, 1995]. The equilibrium evaporation term in equation (3) represents evaporation at the limit of complete decoupling between vegetation surface and atmosphere [*McNaughton and Jarvis*, 1983]. In our previous studies [*Kumagai et al.*, 2004c, 2005], we found large decoupling coefficient values because of relatively large G_s compared with aerodynamic conductance, and that net available energy is the primary forcing variable for evapotranspiration at the studied forest. Thus, the α_{PT} coefficient as a function of s well reflects observations that the LHNP tropical rain forest ecosystem tends to have little regulation of forest water use, despite episodic severe soil drying. This is unlike Eastern Amazonian forests, which tend to show isohydric behavior [*Fisher et al.*, 2006]. In addition, using the nonlinear parameter $q = 3$ [*Kumagai and Porporato*, 2012], we assumed that plants with little regulation of water use can allow their water potential to approach the hydraulic failure threshold without sensing water stress [see *McDowell et al.*, 2008]. Thus, the increment rate of ζ with soil moisture deficit (see equation (4)) for the studied vegetation can be taken as a relatively strong nonlinear increase [*Porporato et al.*, 2001].

[25] Roots concentrate in a soil depth less than 0.5 m (T. Kume, personal observation, 2008). Principal soil moisture dynamics are mainly the result of root water absorption to a depth around 1.0 m, as supported by findings from a soil penetration test (T. Wakahara, personal observation, 2008). Thus, we assumed a Z_r of 1.0 m for LHNP. The parameters n and s_h, corresponding to saturated and residual water contents, respectively, were estimated using the soil water retention curve obtained in the field [*Kumagai et al.*, 2004a, 2004b].

[26] The Ultisols at LHNP have a very high sand content, and therefore act like sand in terms of water movement at high soil matric potential. However, they retain water like clay soils at lower potential [*Kumagai et al.*, 2004c]. In fact, K_{sat} and β at this site, which were estimated using nonlinear least squares regression between the time courses of s by numerical solution of equation (1) and the observations [*Kumagai et al.*, 2004a, 2004b], are typical for sandy clay–silty clay loam and sand, respectively [see *Campbell and Norman*, 1998].

[27] s_{fc} was assumed to be s when $L(s)$ in χ in equation (1) ($=L(s) + E(s, t)$) could not be ignored, and thus $L(s) = K(s) =$ 0.1 mm day^{-1}. Also, values of s_h and s_W were estimated using the $s - \alpha_{PT}$ relationship [*Kumagai et al.*, 2004a, 2004b]. Since there was no evapotranspiration plateau at high s at the site, s^* was assumed equal to s_{fc}.

[28] Mean daily R_n values in wet and dry seasons were obtained; in LHNP, R_n in the wet season (October–May) is lower than that in the dry season (April–September), owing to cloud cover effects.

[29] Throughfall and stemflow only occur when rainfall exceeds certain thresholds, and can be described as linear functions of rainfall. Consequently, daily interception loss was related to incident rainfall in a single storm event by

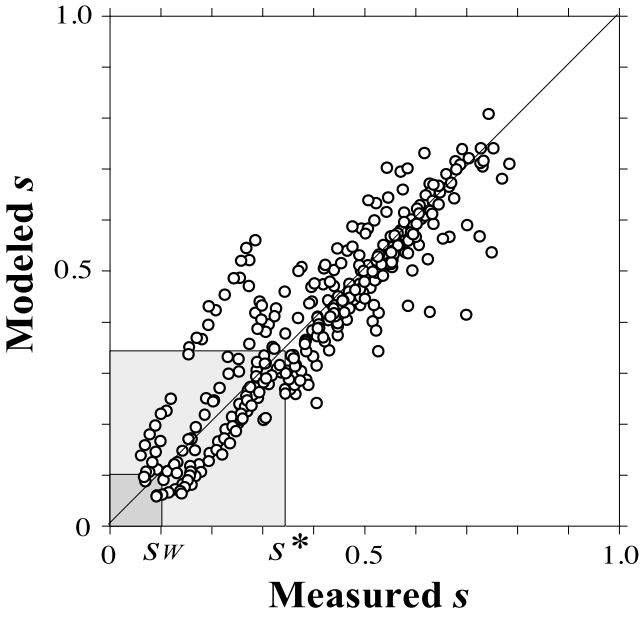

Figure 1. Comparison between measured and modeled relative soil moisture (s). Dark and light shaded areas denote drought conditions below s at plant wilting point (s_W) and s at plant stress point (s^*), respectively. 1:1 line is also presented.

subtracting both the throughfall and stemflow functions from rainfall in LHNP [*Manfroi et al.*, 2006]. Thus, Δ, the amount of rainfall that can accumulate on forest canopy during a rainfall event, was calculated from the daily interception functions of rainfall.

[30] Using the model parameters for present vegetation and time series of rainfall as local forcing data, the soil moisture balance model (equation (1)) was validated in a deterministic mode (i.e., without use of probabilistic descriptions). As a result, we found that the model reproduced well the measured s, including under severe drought conditions (Figure 1). This was despite all simplifying assumptions, such as the use of averaged R_n for calculating evapotranspiration (equation (3)). The figure reveals that modeled and measured s were not significantly different (P = 0.37, slope = 1.01, R^2 = 0.80). Again, soil moisture dynamics is a main determinant of hydrologic fluxes in this model, and thus the validation of measured s time series should be sufficient. Also, in the context of s model validation, we confirmed that model estimation of total annual evapotranspiration was consistent with measurements ($\sim$1400 mm year^{-1}, provided by *Kumagai et al.* [2004a]).

3.2. Rainfall Characteristics

[31] Mean annual rainfall was around 2740 mm at Miri Airport, 20 km from LHNP, for the period 1968–2001, whereas in LHNP it was around 2600 mm for 2000–2006. This small spatial difference in mean annual rainfall was not detected in 0.25° resolution Tropical Rainfall Measuring Mission (TRMM) 3B42 data for 2000–2009 (data not shown). Thus, we assumed that we could substitute the long-term rainfall record at Miri Airport for that at LHNP. This rainfall record shows significant interannual rainfall variability in the region. For example, maximum and minimum annual rainfalls for 1968–2001 were 3499 mm in 1988 and 2125 mm in 1976, respectively. Although the study site is in a region with one of the smallest seasonal rainfall variations in the world [see *Kumagai et al.*, 2005, Figure 3], there is a slight seasonal cycle. It is drier from February to September, and wetter from October to January [see *Kumagai et al.*, 2009, Figure 1a].

[32] In the tropical part of the Indian monsoon area, dry spells of 15–30 days are not uncommon [*Yasunari*, 1979]. To identify severe droughts, we calculated a 30-day shifting average of rainfall, based on daily data at Miri for the period 1968–2001 (Figure 2). This calculation was based on the method of *Duchon* [1979], who forwarded the time series requirement to analyze the rainfall cycle at a period shorter than half a year [see *Kumagai et al.*, 2005, Figure 3], and *Sakai et al.* [2006], who indicated that a dry period of at least 30 days is most closely linked to drought stemming from ecohydrological aspects like regional soil moisture dynamics

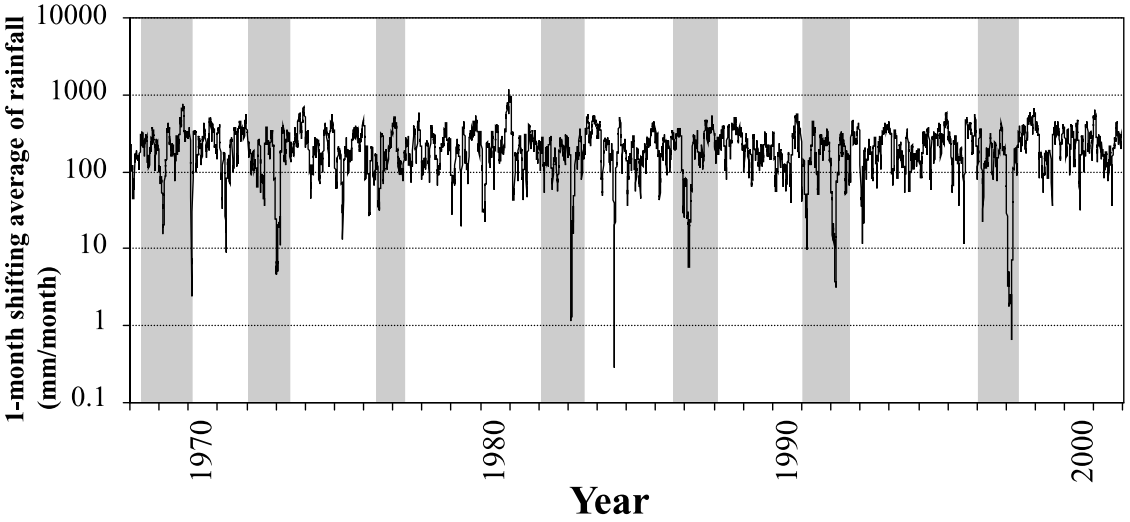

Figure 2. Time series of one-month shifting average of daily rainfall at Miri. Shaded columns represent periods of El Niño events.

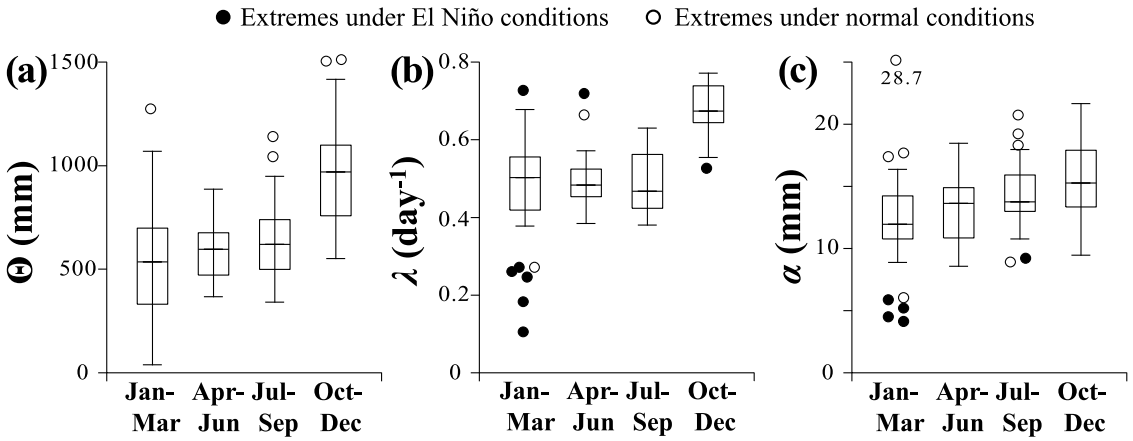

Figure 3. Box plots of (a) total seasonal rainfall (Θ), (b) estimated seasonal rate of arrival of rainfalls (λ), and (c) seasonal average rainfall depth (α), based on daily data of rainfall at Miri. Observations are shown for more than 1.5 interquartile ranges, under El Niño (closed circles) and normal (open circles) conditions. One outlier in Figure 3c is indicated by its value.

and plant water relations. The results show that there were sporadic but severe dry spells with persistence of at least 30 days, which typically corresponded with El Niño events defined by Sea Surface Temperature (SST) anomaly from 5°S–5°N and 150°W–90°W.

[33] To assess drought-induced mortality for each dry and wet season, we also evaluated the primary forcing terms of the stochastic ecohydrological model, i.e., the arrival rate of rainfalls λ and rainfall depth α, for each season. Seasons are typically represented by sequences of three months, i.e., December–February, March–May, June–August and September–November. However, three-month seasonal means of Θ, λ and α using the above representations could not sufficiently describe their seasonal variations. Thus, we computed time series of total precipitation (Θ: mm), λ and α over the period 1968–2001, for each of the four seasons, January–March, April–June, July–September and October–December. In this way, variances of yearly time series of seasonal averaged values (Θ, λ and α) were maximized. We defined interannual and seasonal variations in rainfall characteristics using box plots for Θ, λ and α (Figure 3). On average, all rainfall parameters had slight seasonal variations. Outliers, and thus interannual variations, were especially prominent from January–March. Furthermore, as stated previously, severe drought conditions were generally present during El Niño events (Figure 3).

[34] The effects of interannual climate fluctuations were then incorporated into the index η, using the time series of λ and α obtained for each season. Fluctuations of these parameters are represented by gamma distributions based on their means and standard deviations, and are obtained from the respective yearly time series (Table 2). For each season, steady state η are calculated with pairs of λ and α generated by Monte Carlo sampling, using gamma distributions [*D'Odorico et al.*, 2000; *Porporato et al.*, 2006; *Kumagai et al.*, 2009].

3.3. High Mortality Under a Severe Drought Condition Associated With 1997–1998 El Niño

[35] The forests of LHNP experienced a severe drought associated with the 1997–1998 El Niño, and drought-induced mortality increase was observed [*Nakagawa et al.*, 2000; *Potts*, 2003]. To examine usefulness of Tree Death Index η for the LHNP tropical rain forest, we used the results of *Nakagawa et al.* [2000], summarized as follows.

[36] The strong 1982–1983 El Niño caused very severe drought. However, the 1997–1998 El Niño was the strongest in the 20th century, and its associated drought was the most severe (statistically, the Kolmogorov-Smirnov test showed that a drought such as in 1998 may occur once in about 360 years) (see Figure 2). Mortality rates during that drought were 6.37% year^{-1}, as compared with 0.89% year^{-1} during the pre-drought period (1993–1997); the basal area lost during the drought was 3.4 times that of the annual increase in basal area during the pre-drought. Notably, the dominant family in the study forest, Dipterocarpaceae, had a 12–30 times higher in the drought than the pre-drought period. The mortalities shown here are among the highest ever observed in world tropical rain forests [*Phillips et al.*, 2010].

3.4. GCM Projections of Rainfall in Late 21st-Century

[37] Rainfall characteristics for the late 21st century (2080–2099) scenario were taken from model outputs at approximate coordinates 4°12′N, 114°02′E, simulated by 14 IPCC GCMs (listed in Table 3), available through a public website (http://www.ipcc-data.org/). The GCM runs used here follow the Special Report on Emissions Scenarios (SRES) A2 [*Nakicenovic et al.*, 2000], which assumes a very heterogeneous world with continuously increasing population and regionally oriented economic growth that is more fragmented and slower than in other storylines. There are

Table 2. Total Seasonal Rainfall (Θ), Mean Yearly Rate of Arrival of Rainfalls (λ), Rainfall Depth (α), and Standard Deviations, for Each Season of 1968–2001 in Lambir Hills National Park

Season	Θ (mm)	λ (day^{-1})	α (mm)
January–March	541.3 ± 279.9	0.47 ± 0.15	12.0 ± 4.5
April–June	583.3 ± 136.9	0.49 ± 0.075	13.1 ± 2.6
July–September	642.5 ± 183.2	0.49 ± 0.080	14.2 ± 2.7
October–December	973.5 ± 241.2	0.68 ± 0.064	15.5 ± 3.1

Table 3. Total Seasonal Rainfall (Θ), Mean Yearly Rate of Arrival of Rainfalls (λ), and Rainfall Depth (α) for Each Season at Lambir Hills National Park, from Global Climate Model (GCM) Simulations for the Period 2080–2099[a]

GCM	Parameter	January–March	April–June	July–September	October–December
14 GCM average[b]	Θ[c] (mm)	508.0 (63.6)	605.2 (89.3)	699.2 (96.5)	1082.6 (121.8)
14 GCM average	λ (day^{-1})	0.46	0.50	0.51	0.70
14 GCM average	α (mm)	11.6	13.4	14.8	16.7
HADCM3	Θ (mm)	371.1	450.2	631.3	1016.7
HADCM3	λ (day^{-1})	0.40	0.44	0.49	0.69
HADCM3	α (mm)	9.8	11.3	14.0	16.0

[a]All values were taken as relative changes in rainfall predicted by each GCM, but offset by changes to rainfall observed in 1968–2001, according to *Malhi et al.* [2009].
[b]14 Intergovernmental Panel on Climate Change (IPCC) GCMs used: NCPCM, NCCCSM, MRCGCM, MPEH5, MIMR, IPCM4, INCM3, GIER, GFCM21, GFCM20, ECHOG, CSMK3, CNCM3, and HADCM3 (see http://www.ipcc-data.org/).
[c]Standard deviations of Θ simulated from 14 GCMs are shown in parentheses.

well-known uncertainties regarding comparison of point-scale field observations to the coarse-resolution GCM grid cell [*Miralles et al.*, 2010]. Here, specific values projected by each GCM are not important, unlike the variance and mean of the values. In addition, topography of the study site is widespread lowland, and climatic factors might be somewhat homogeneous within the GCM grid cell. Therefore, we assumed that the difference between point-scale observations and grid cell-scale simulations was included in the GCM-to-GCM variation of projected value, and there was no correction for this difference in each projection.

[38] Based on an assumption that GCM simulations capture future seasonal changes in relative rainfall intensity in spite of their current tendency to underestimate absolute rainfall, we followed *Malhi et al.* [2009] and accepted relative changes in rainfall predicted by each GCM, but offset them using rainfall observed from 1968 to 2001:

$$\Theta_{21}(m,j) = \Theta_{\mathrm{obs\_20}}(m)\left(1 + \frac{\Theta_{\mathrm{GCM\_21}}(m,j) - \Theta_{\mathrm{GCM\_20}}(m,j)}{\Theta_{\mathrm{GCM\_20}}(m,j)}\right), \tag{12}$$

where m and j denote a season and a GCM, respectively. Subscripts 21, obs_20, GCM_20 and GCM_21 denote an objective value for the late 21st century (2080–2099), observations in the late 20th century (1968–2001), and GCM-simulations for the late 20th (1961–1990) and 21st (2080–2099) centuries, respectively. $\Theta_{\mathrm{GCM\_20}}$ is GCM-simulated rainfall under Non-SRES 20C3M assuming increasing greenhouse gases, as observed through the 20th century. The future rainfall parameters λ_{21} and α_{21} were calculated using tuning parameter a obtained to minimize b, given by

$$b = T_{seas}\alpha_{\mathrm{obs\_20}}\lambda_{\mathrm{obs\_20}}\left(1 + \frac{\Theta_{\mathrm{GCM\_21}} - \Theta_{\mathrm{GCM\_20}}}{\Theta_{\mathrm{GCM\_20}}}\right) - T_{seas}\alpha_{21}\lambda_{21}, \tag{13}$$

in which

$$\alpha_{21} = \alpha_{\mathrm{obs\_20}} + a\sigma_{\alpha} \tag{14}$$

$$\lambda_{21} = \lambda_{\mathrm{obs\_20}} + a\sigma_{\lambda} \tag{15}$$

where σ_{α} and σ_{λ} are standard deviations of $\alpha_{\mathrm{obs\_20}}$ and $\lambda_{\mathrm{obs\_20}}$, respectively. Here, we assumed that λ_{21} and α_{21} vary linearly with each slope of σ_{α} and σ_{λ} between GCM-simulated Θ values.

[39] With the revised calculation using equation (12), many GCM simulations show a tendency in the late 21st century for increased seasonality in Θ, i.e., a wet season becomes wetter, and a dry season drier (Tables 2 and 3). On the other hand, HADCM3 showed the most severe change in rainfall regime, projecting dry seasons to become much drier, with little change in the wet season. HADCM3 has a different model weighting, based on capturing interannual variability, and has many advantages in projecting climate-induced drought; thus, this extreme simulation result is likely [*Malhi et al.*, 2009]. Hence, we constructed two types of future scenarios for 2080–2099, outputs averaged over 14 GCM simulations and from HADCM3 only (Table 3). Here, we assumed that the different periods, for observations (1968–2001) and GCM runs (1961–1990), can represent late 20th century precipitation characteristics, and that the GCM runs for the late 21st (model period 2080–2099) can be compared with observations of different period duration (1968–2001), because model outputs were translated to PDFs through the stochastic treatments. Again, interannual variations in the parameters λ_{21} and α_{21} are represented by gamma distributions using σ_{λ} and σ_{α}, respectively. For each season, steady state η under future climate conditions were calculated with the pairs of λ_{21} and α_{21} generated by Monte Carlo sampling, using gamma distributions.

4. Results

[40] Interannual variation in steady state η for each season is shown in Figure 4. Although mean η for January–March, April–June and July–September do not have significant differences (around 0.07; Figures 4a–4c), interannual rainfall fluctuation in January–March (Figure 3) appreciably increases the frequency of higher η values (referred to as the "fatal mode" of η, because mortality might be higher under conditions with such high η values) (Figure 4a). Notably, the atom of probability at $\eta = 1$ in January–March reaches 10.0% (Figure 4a). On the other hand, mean η in October–December is around 0.01, and about 85% of its frequency is below 0.01 (Figure 4d). The steady state η estimated under the El Niño conditions of 1997–1998 were around the mean, or at the boundary of at least 35% of the upper tail of the PDF of η, $pdf(\eta)$ for April–June, July–September and October–December (Figures 4b–4d). For January–March it was one, representing the most fatal situation (Figure 4a).

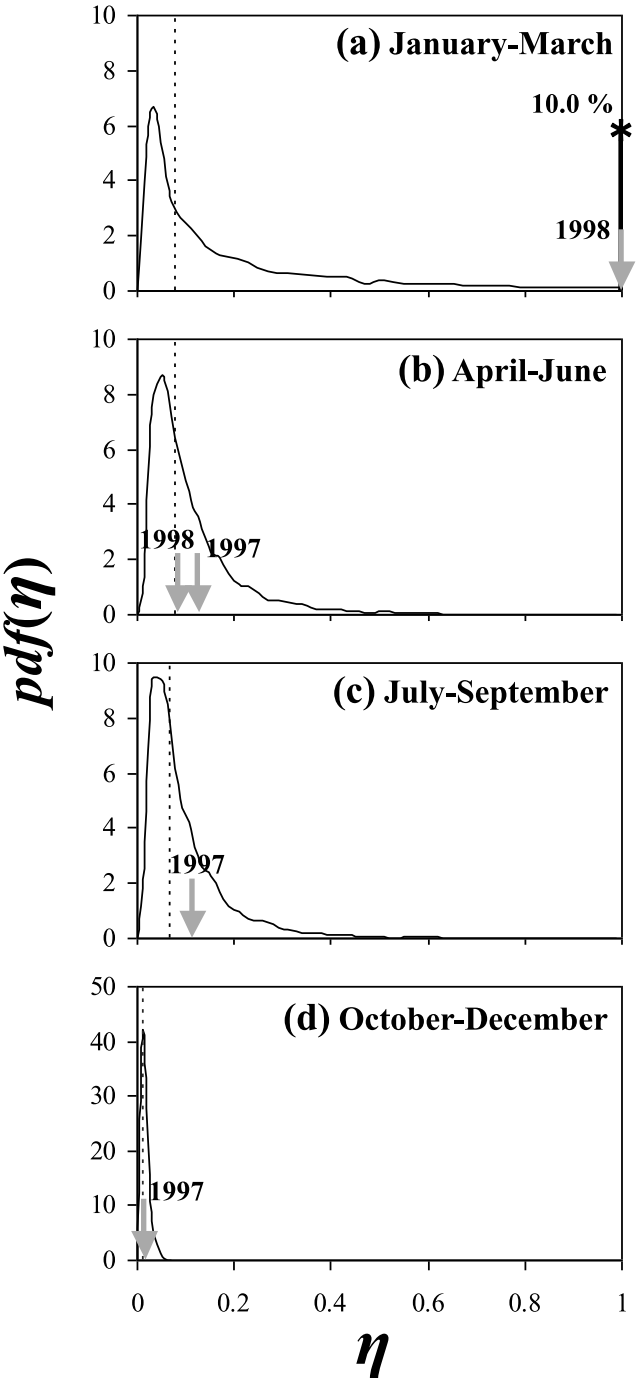

Figure 4. Probability density function of Tree Death Index η, ($pdf(\eta)$), considering interannual variations in rainfall parameters λ and α from 1968 to 2001, for (a) January–March, (b) April–June, (c) July–September, and (d) October–December. Vertical dotted line represents mean η for each season. Asterisk represents atom of probability at $\eta = 1$. Arrows with numbers represent values of η estimated under El Niño conditions of 1997–1998.

[41] Figure 5 compares interannual variations in the steady state η for each season in the late 20th century, and projected for the late 21st century. Owing to appreciable reduction in rainfall in January–March under the GCM rainfall

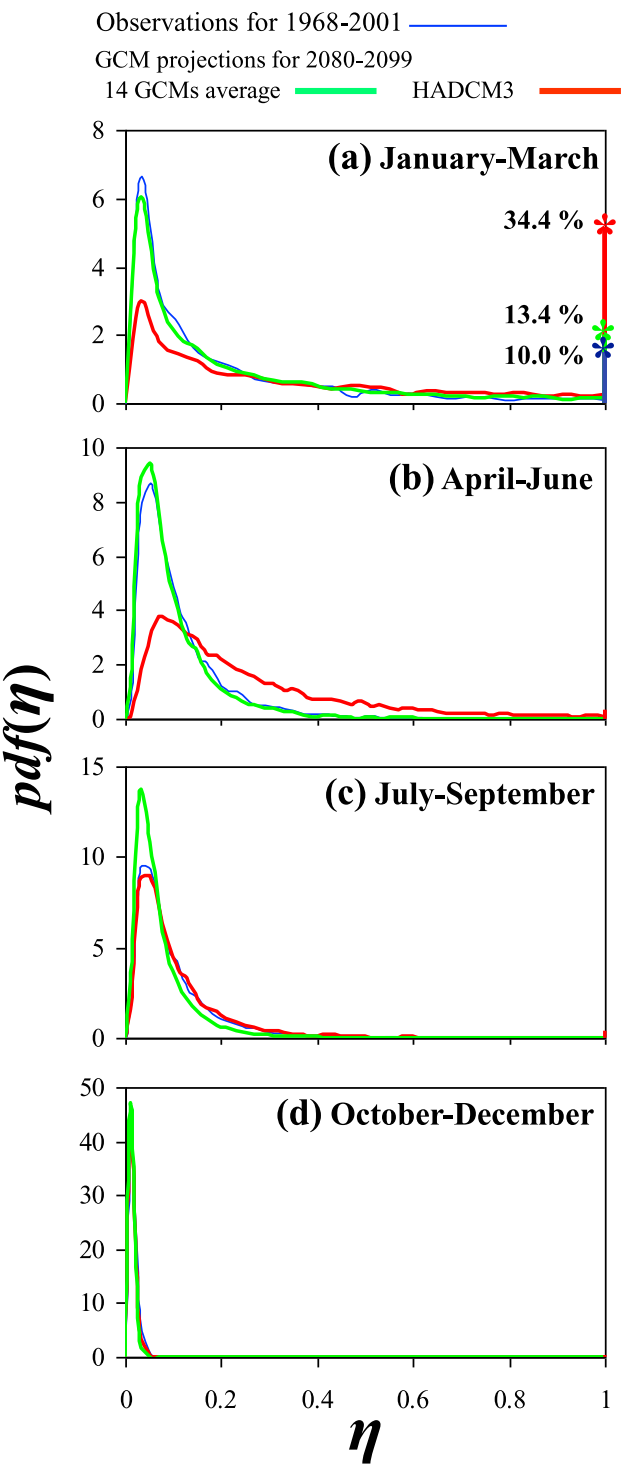

Figure 5. Probability density function of Tree Death Index η, ($pdf(\eta)$), describing its interannual variation for (a) January–March, (b) April–June, (c) July–September, and (d) October–December, estimated using projected rainfall parameters for 2080–2099 obtained from GCMs simulations (Table 3). Asterisks represent atoms of probabilities at $\eta = 1$. As a reference, corresponding $pdf(\eta)$ lines calculated using rainfall parameters from 1968 to 2001 are also represented (thin curves).

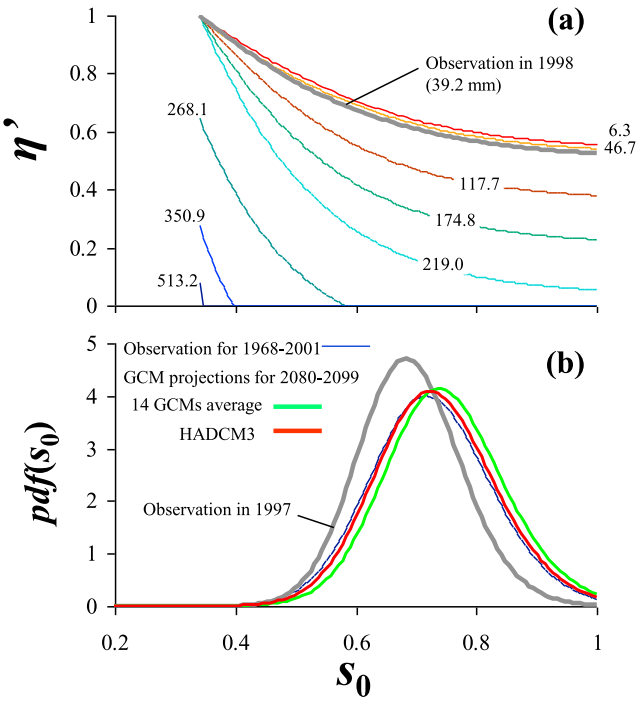

Figure 6. (a) Tree Death Index affected by preceding wet season water storage (η') during January–March, as a function of soil moisture value at beginning of October–December (s_0) and (b) probability density function of relative soil moisture ($pdf(s_0)$) for October–December. In Figure 6a, lines are for different seasonal total rainfall in January–March, represented by numbers (mm) on or beside them. Each rainfall amount of 513.2, 350.9, 268.1, 219.0, 174.8, 117.7, 46.7 and 6.3 mm corresponds to $a = 0$, -0.5, -0.8, -1.0, -1.2, -1.5, -2.0 and -2.5, respectively (see equations (14) and (15)).

projections, especially that of HADCM3, the frequencies of η fatal mode and atoms of probabilities at $\eta = 1$ significantly increase in the 21st century (Figure 5a). The PDFs of η for April–June and July–September are almost the same in calculations for the 20th century. Compared with the 20th century simulations, the rainfall decrease in April–June in the HADCM3 simulation (Tables 2 and 3) increases the frequency of greater η (Figure 5b), and the rainfall increases in July–September in the projection by the 14 GCM average (Tables 2 and 3) augments contributions to small η and decreases large η (Figure 5c). In October–December, moister environments projected for the 21st century do not significantly alter $pdf(\eta)$ (Figure 5d).

[42] The study site has slight seasonality in rainfall (Table 2), and the GCMs projected that this seasonality will amplify in the late 21st century (Table 3). Here, higher η appear in January–March, the driest season (Figures 4 and 5), and the preceding October–December is the moistest season of the year. Thus, it is logical to expect that soil water storage in October–December affects η in the following January–March, and this effect will be modified by climate change. The extended definition of η accounting for the high soil moisture at the start of the preceding season (η': equation (11)), for different total seasonal rainfall in January–March (Θ_{JFM}), are calculated using rainfall parameters λ_{21} and α_{21} obtained from $\Theta_{JFM} = T_{seas}\lambda_{21}\alpha_{21}$ and equations (14) and (15) (Figure 6a). The η' has a maximum value at s^*, equal to the steady state η (see equation (11)), and decreases with increasing s_0. As Figure 6a shows, η' can reach one when $\Theta_{JFM} < 200$ mm, shows little difference when $\Theta_{JFM} < 50$ mm, and has a lower value with average climate conditions in January–March, i.e., $\Theta_{JFM} = 513.2$ mm. In addition, $pdf(s_0)$ for October–December in Figure 6b shows that whereas there is little difference between soil moisture conditions in the 20th century and the HADCM3 projection, increased rainfall in the projection by the 14 GCM average increases the frequency of greater s, and that the study site under El Niño conditions in 1997 experienced very dry conditions compared with normal.

[43] Here, using Figures 6a and 6b, we compute the mean total η' in January–March, taking into consideration the effect of water storage in the preceding October–December as $\overline{\eta'}_{JFM} = \int_0^1 \eta'_{JFM} pdf_{OND}(s_0) ds_0$ (where η'_{JFM} and $pdf_{OND}(s_0)$ define η' in January–March as a function of s_0 and $pdf(s)$ in October–December, respectively). Figure 7 plots $\overline{\eta'}_{JFM}$ against Θ_{JFM}. The $\overline{\eta'}_{JFM}$ abruptly increases when $\Theta_{JFM} < 270$ mm, and reaches a plateau and maximum (around 0.64) when $\Theta_{JFM} < 50$ mm. It is interesting that the $\overline{\eta'}_{JFM}$ calculated using rainfall parameters under El Niño conditions in 1998 lies on the plateau (Figure 7). In Figure 7, we indicate possible ranges of Θ_{JFM} obtained from 1968 to 2001 observation and GCM projections for 2080–2099. This shows that while the maximum value of $\overline{\eta'}_{JFM}$ in 1998 is somewhat an outlier when considering the Θ_{JFM} in 1968–

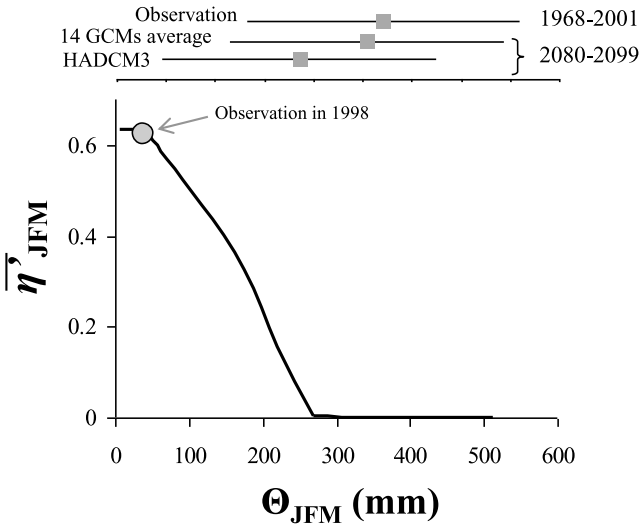

Figure 7. Mean total Tree Death Index in January–March ($\overline{\eta'}_{JFM}$), considering effect of water storage in preceding October–December (s_0) as a function of total seasonal rainfall in January–March (Θ_{JFM}). Also shown is $\overline{\eta'}_{JFM}$, calculated using rainfall parameters obtained from observations under El Niño conditions in 1998. Mean Θ_{JFM} and standard deviations in late 20th century (observations from 1968 to 2001) and late 21st century (projections for 2080–2099 by the 14 GCM average and HADCM3) are shown at the top.

2001, such a high $\overline{\eta'}_{JFM}$ is more likely to occur in the late 21st century, especially in the HADCM3 projection.

5. Discussion and Conclusions

[44] Using a combination of field measurements and theoretical considerations, the index for drought-induced tree mortality (Tree Death Index η), associated with a stochastic ecohydrological model and GCM projections of rainfall, allows us to examine how future rainfall shifts will affect ecosystem water budgets and related drought-induced mortality of a Bornean tropical rain forest. The concept of η is close to a water stress integral (WSI) involving temporal accumulation of deviation in leaf water potentials relative to the maximum observed value, providing a long-term index of plant water stress [*Myers*, 1988]. *Nepstad et al.* [2007] effectively explained the drought-induced death and survivorship of trees in a large throughfall exclusion experiment, using the WSI. Unlike the WSI, the η model has as its primary forcing terms rainfall statistics, which describe the impact of global-change-type drought.

[45] The field measurements permitted derivation of realistic relationships that link the rainfall forcing term generated from historical data and GCM projections with ecosystem water cycling, including tree water stress. For example, field data were used to derive relationships between transpiration and extractable soil water content, and between rainfall and interception, seasonal evaporative demand, and drainage flow parameters [e.g., *Kumagai et al.*, 2004b, 2009]. As a result, we could describe ecosystem water cycling using the parameters (Table 1), and formulate a hypothesis about the relationship between plant water stress and soil moisture.

[46] Mechanistic or semi-mechanistic modeling of tree death [e.g., *Martínez-Vilalta et al.*, 2002; *Fisher et al.*, 2010] has received less attention, mainly because of sparse data on the relationship between environmental conditions and tree health [*Keane et al.*, 2001]. Our present ability to determine emergence of global changes in forest mortality is constrained by a lack of systematic global monitoring [*Allen et al.*, 2010]. Widely used empirical mortality models [e.g., *Bugmann and Solomon*, 2000; *Horner et al.*, 2009] are effective for current climatic conditions but are likely inadequate for future climate change conditions, because they lack insight into the relationship between changing environmental factors and responding physiological mechanisms. Improvements for mortality modeling problems should include a biologically reasonable predictor in a stochastic algorithm that can account for plant stresses in response to environmental changes [*Hawkes*, 2000].

[47] There are promising indexes for examination of the relationship between climate-induced forest die-off and drought intensity and duration, as follows. Tree mortality abruptly increases when the index exceeds environmental and/or physiological thresholds. Many researchers have used the maximum climatological water deficit (MCWD), defined as the most negative value of monthly precipitation minus monthly evapotranspiration over a year, to explain the drought sensitivity of forest die-off [e.g., *Aragão et al.*, 2007; *Malhi et al.*, 2009; *Phillips et al.*, 2009, 2010]. *Nepstad et al.* [2007] tested the hypothesis that tree mortality increases abruptly during drought, when plant-available soil water (PAW) declines below a critical minimum threshold. They effectively used PAW, which accounts for soil moisture conditions and the ability of different types of access to soil water. The index η was developed here as a simple mechanistic tree mortality model based on ecophysiological (both aboveground and belowground processes) and soil physics properties, and was related to directly measured quantities in the studied forest ecosystem, as well as to stochastic rainfall properties and global climatic events (e.g., El Niño).

[48] Practically, such an index must be translated into actual tree mortality, such as fraction of tree deaths per year. For example, to simulate tree death from carbon starvation, *Fisher et al.* [2010] formulated drought-induced tree mortality (M: % year^{-1}) as a function of stored carbon pool, background mortality (B_m: % year^{-1}), and single cohort mortality rate (S_m: % year^{-1}). In their model, $M = B_m$ and $M = B_m + S_m$ occur when mean cohort carbon storage is equal to leaf biomass, i.e., irrespective of stress on the carbon store, and when carbon storage is zero, respectively. Also, in the ecosystem demography model by *Moorcroft et al.* [2001], mortality rate is calculated as the sum of two terms: an individual's density-independent mortality rate, related to its longevity, and its density-dependent mortality rate, associated with its current net carbon production. The first term could correspond to B_m. These concepts are based on death from carbon starvation, including isohydric behavior in response to drought. Here, drought-induced mortality from hydraulic failure might be similarly modeled as

$$M = B_m + \frac{\eta}{\eta_{\max}} S_m, \tag{16}$$

where $\eta_{\max}$ is the possible maximum value of η, and S_m is the value when η is $\eta_{\max}$. Note that $M = B_m$ occurs when $\eta = 0$, i.e., irrespective of the hydraulic failure. This modeled M increases linearly with η, but η is a nonlinear function of ecophysiological and environmental factors.

[49] Further, generalization of η modeling, such as its application to other sites or creation of global η maps, is needed for predicting the extent and patterns of future alteration in forests affected by drought-induced mortality. For example, using daily precipitation values on a global 0.25° latitude-longitude resolution grid from the National Centers for Environmental Prediction–National Center for Atmospheric Research (NCEP–NCAR) reanalysis [see *Kistler et al.*, 2001], we can obtain global and temporal patterns of precipitation statistics, i.e., α and λ, which drive the stochastic soil moisture and η model. Global assessments of evapotranspiration characteristics, e.g., validation and parameterization, could be done using tower eddy covariance and meteorological data from the FLUXNET data archive (http://www.fluxnet.ornl.gov/). Also, the relationship between evapotranspiration and soil moisture could be obtained from combination of the FLUXNET data and outputs from the Second Global Soil Wetness Project (GSWP-2) [see *Dirmeyer et al.*, 2006]. Also needed are an improved network of observations, e.g., a global network of sap flow measurements for drought physiology, and global and annual maps of actual tree mortality (M) [see *Allen et al.*, 2010] for translating the η map to an M map.

[50] We found that future rainfall shifts cause higher and lower frequencies of the fatal mode of η in January–March and October–December, respectively (Figure 5). This

finding is attributed to a projected reduction and increase in rainfall in January–March and October–December, respectively. Thus, we examined the effect of a projected increase in soil water storage in October–December on tree water stress the following January–March (Figure 6). Despite the stored water effect, the computed η for January–March 1998 (strong ENSO event) reached the maximum possible; the likelihood of this η value was found very small in the 20th century (Figure 7). Interannual rainfall variation simulated by the GCMs (especially HADCM3) demonstrated that tree mortality as great as in the 1998 ENSO event is more likely in the late 21st century (Figure 7). Furthermore, *Phillips et al.* [2010] suggested a mortality more sensitive to drought in Bornean forests than in Amazonian forests. This motivates greater consideration of the influence of severe drought on forest mortality in the 20th century at our Borneo study site. More extensive and technically difficult experiments are required to explain the meaning of η in M (see equation (16)) and the applicability of η and M modeling to other forest sites.

[51] **Acknowledgments.** T. K. is grateful to the Forestry Department, Sarawak, for their support during the fieldwork for this study. T. K. also thanks Tohru Nakashizuka, Masakazu Suzuki and Tetsukazu Yahara for their support, and numerous colleagues who helped with this fieldwork. This study was funded by Core Research for Evolutional Science and Technology (CREST) of the Japan Science and Technology Agency (JST), the Global COE (Centers of Excellence) Program (GCOE) of the Japan Society for the Promotion of Science (JSPS), grants from the Ministry of Education, Culture, Sports, Science and Technology, Japan (21255001, 20248016, 20380090 and 19255006), and the Excellent Young Researcher Overseas Visit Program under the sponsorship of the JSPS.

References

Adams, H. D., A. K. Macalady, D. D. Breshears, C. D. Allen, N. L. Stephenson, S. R. Saleska, T. E. Huxman, and N. G. McDowell (2010), Climate-induced tree mortality: Earth system consequences, *Eos Trans. AGU*, *91*(17), 153–154, doi:10.1029/2010EO170003.

Allen, C. D., et al. (2010), A global overview of drought and heat-induced tree mortality reveals emerging climate change risk for forests, *For. Ecol. Manage.*, *259*, 660–684, doi:10.1016/j.foreco.2009.09.001.

Aragão, L. O. C., Y. Malhi, R. M. Roman-Cuesta, S. Saatchi, L. O. Anderson, and Y. E. Shimabukuro (2007), Spatial patterns and fire response of recent Amazonian droughts, *Geophys. Res. Lett.*, *34*, L07701, doi:10.1029/2006GL028946.

Avissar, R., and D. Werth (2005), Global teleconnections resulting from tropical deforestation, *J. Hydrometeorol.*, *6*, 134–145, doi:10.1175/JHM406.1.

Betts, R. A., P. M. Cox, M. Collins, P. P. Harris, C. Huntingford, and C. D. Jones (2004), The role of ecosystem-atmosphere interactions in simulated Amazonian precipitation decrease and forest dieback under global climate warming, *Theor. Appl. Climatol.*, *78*, 157–175, doi:10.1007/s00704-004-0050-y.

Bonan, G. B. (2008), Forests and climate change: Forcing, feedbacks, and the climate benefits of forests, *Science*, *320*, 1444–1449, doi:10.1126/science.1155121.

Breshears, D. D., et al. (2005), Regional vegetation die-off in response to global-change-type drought, *Proc. Natl. Acad. Sci. U. S. A.*, *102*, 15,144–15,148, doi:10.1073/pnas.0505734102.

Breshears, D. D., O. B. Myers, C. W. Meyer, F. J. Barnes, C. B. Zou, C. D. Allen, N. McDowell, and W. T. Pockman (2009), Tree die-off in response to global change-type drought: Mortality insights from a decade of plant water potential measurements, *Front. Ecol. Environ.*, *7*, 185–189, doi:10.1890/080016.

Bugmann, H. K. M., and A. M. Solomon (2000), Explaining forest composition and biomass across multiple biogeographical regions, *Ecol. Appl.*, *10*, 95–114, doi:10.1890/1051-0761(2000)010[0095:EFCABA]2.0.CO;2.

Campbell, G. S., and J. M. Norman (1998), *An Introduction to Environmental Biophysics*, 2nd ed., Springer, New York, doi:10.1007/978-1-4612-1626-1.

Canadell, J. G., C. Le Quere, M. R. Raupach, C. B. Field, E. T. Buitenhuis, P. Ciais, T. J. Conway, N. P. Gillett, R. A. Houghton, and G. Marland (2007), Contributions to accelerating atmospheric CO_2 growth from economic activity, carbon intensity, and efficiency of natural sinks, *Proc. Natl. Acad. Sci. U. S. A.*, *104*, 18,866–18,870, doi:10.1073/pnas.0702737104.

Damesin, C. (2003), Respiration and photosynthesis characteristics of current-year stems of *Fagus sylvatica*: From the seasonal pattern to an annual balance, *New Phytol.*, *158*, 465–475, doi:10.1046/j.1469-8137.2003.00756.x.

Dirmeyer, P. A., X. Gao, M. Zhao, Z. Guo, T. Oki, and N. Hanasaki (2006), GSWP-2: Multi-model analysis and implications for our perception of the land surface, *Bull. Am. Meteorol. Soc.*, *87*, 1381–1397, doi:10.1175/BAMS-87-10-1381.

D'Odorico, P., L. Ridolfi, A. Porporato, and I. Rodriguez-Iturbe (2000), Preferential states of seasonal soil moisture: The impact of climate fluctuations, *Water Resour. Res.*, *36*(8), 2209–2219, doi:10.1029/2000WR900103.

Duchon, C. E. (1979), Lanczos filtering in one and two dimensions, *J. Appl. Meteorol.*, *18*, 1016–1022, doi:10.1175/1520-0450(1979)018<1016:LFIOAT>2.0.CO;2.

Field, C. B., M. J. Behrenfeld, J. T. Randerson, and P. Falkowski (1998), Primary production of the biosphere: Integrating terrestrial and oceanic components, *Science*, *281*, 237–240, doi:10.1126/science.281.5374.237.

Fisher, R. A., M. Williams, R. L. do Vale, A. L. da Costa, and P. Meir (2006), Evidence from Amazonian forests is consistent with isohydric control of leaf water potential, *Plant Cell Environ.*, *29*, 151–165, doi:10.1111/j.1365-3040.2005.01407.x.

Fisher, R., N. McDowell, D. Purves, P. Moorcroft, S. Sitch, P. Cox, C. Huntingford, P. Meir, and F. I. Woodward (2010), Assessing uncertainties in a second-generation dynamic vegetation model caused by ecological scale limitations, *New Phytol.*, *187*, 666–681, doi:10.1111/j.1469-8137.2010.03340.x.

Grace, J., Y. Malhi, N. Higuchi, and P. Meir (2001), Productivity of tropical forests, in *Terrestrial Global Productivity*, edited by J. Roy et al., pp. 401–426, Academic, San Diego, Calif., doi:10.1016/B978-012505290-0/50018-1.

Hawkes, C. (2000), Woody plant mortality algorithms: Description, problems and progress, *Ecol. Modell.*, *126*, 225–248, doi:10.1016/S0304-3800(00)00267-2.

Horner, G. J., P. J. Baker, R. MacNally, S. C. Cunningham, J. R. Thomson, and F. Hamilton (2009), Mortality of developing floodplain forests subjected to a drying climate and water extraction, *Global Change Biol.*, *15*, 2176–2186, doi:10.1111/j.1365-2486.2009.01915.x.

Houghton, R. A., and J. L. Hackler (1999), Emissions of carbon from forestry and land-use change in tropical Asia, *Global Change Biol.*, *5*, 481–492, doi:10.1046/j.1365-2486.1999.00244.x.

Intergovernmental Panel on Climate Change (2007), *Climate Change 2007: Impacts, Adaptation and Vulnerability. Contribution of Working Group II to the Fourth Assessment Report of the Intergovernmental Panel on Climate Change*, Cambridge Univ. Press, New York.

Kanae, S., T. Oki, and K. Musiake (2001), Impact of deforestation on regional precipitation over the Indochina Peninsula, *J. Hydrometeorol.*, *2*, 51–70, doi:10.1175/1525-7541(2001)002<0051:IODORP>2.0.CO;2.

Keane, R. E., M. Austin, C. Field, A. Huth, M. J. Lexer, D. Peters, A. Solomon, and P. Wyckoff (2001), Tree mortality in gap models: Application to climate change, *Clim. Change*, *51*, 509–540, doi:10.1023/A:1012539409854.

Kelliher, F. M., R. Leuning, M. R. Raupach, and E.-D. Schulze (1995), Maximum conductances for evaporation from global vegetation types, *Agric. For. Meteorol.*, *73*, 1–16, doi:10.1016/0168-1923(94)02178-M.

Kistler, R., et al. (2001), The NCEP-NCAR 50-year reanalysis: Monthly means CD-ROM and documentation, *Bull. Am. Meteorol. Soc.*, *82*, 247–267, doi:10.1175/1520-0477(2001)082<0247:TNNYRM>2.3.CO;2.

Kumagai, T., and A. Porporato (2012), Strategies of a Bornean tropical rainforest water use as a function of rainfall regime: Isohydric or anisohydric?, *Plant Cell Environ.*, *35*, 61–71, doi:10.1111/j.1365-3040.2011.02428.x.

Kumagai, T., G. G. Katul, A. Porporato, T. M. Saitoh, M. Ohashi, T. Ichie, and M. Suzuki (2004a), Carbon and water cycling in a Bornean tropical rainforest under current and future climate scenarios, *Adv. Water Resour.*, *27*, 1135–1150, doi:10.1016/j.advwatres.2004.10.002.

Kumagai, T., G. G. Katul, T. M. Saitoh, Y. Sato, O. J. Manfroi, T. Morooka, T. Ichie, K. Kuraji, M. Suzuki, and A. Porporato (2004b), Water cycling in a Bornean tropical rain forest under current and projected precipitation scenarios, *Water Resour. Res.*, *40*, W01104, doi:10.1029/2003WR002226.

Kumagai, T., T. M. Saitoh, Y. Sato, T. Morooka, O. J. Manfroi, K. Kuraji, and M. Suzuki (2004c), Transpiration, canopy conductance and the decoupling coefficient of a lowland mixed dipterocarp forest in Sarawak,

Borneo: Dry spell effects, *J. Hydrol.*, *287*, 237–251, doi:10.1016/j.jhydrol.2003.10.002.

Kumagai, T., T. M. Saitoh, Y. Sato, H. Takahashi, O. J. Manfroi, T. Morooka, K. Kuraji, M. Suzuki, T. Yasunari, and H. Komatsu (2005), Annual water balance and seasonality of evapotranspiration in a Bornean tropical rainforest, *Agric. For. Meteorol.*, *128*, 81–92, doi:10.1016/j.agrformet.2004.08.006.

Kumagai, T., N. Yoshifuji, N. Tanaka, M. Suzuki, and T. Kume (2009), Comparison of soil moisture dynamics between a tropical rainforest and a tropical seasonal forest in Southeast Asia: Impact of seasonal and year-to-year variations in rainfall, *Water Resour. Res.*, *45*, W04413, doi:10.1029/2008WR007307.

Laio, F., A. Porporato, C. P. Fernandez-Illescas, and I. Rodriguez-Iturbe (2001), Plants in water-controlled ecosystems: Active role in hydrologic processes and response to water stress. IV. Discussion of real cases, *Adv. Water Resour.*, *24*, 745–762, doi:10.1016/S0309-1708(01)00007-0.

Laurance, W. F. (1999), Reflections on the tropical deforestation crisis, *Biol. Conserv.*, *91*, 109–117, doi:10.1016/S0006-3207(99)00088-9.

Lean, J., and D. A. Warrilow (1989), Simulation of the regional climatic impact of Amazonian deforestation, *Nature*, *342*, 411–413, doi:10.1038/342411a0.

Linton, M. J., J. S. Sperry, and D. G. Williams (1998), Limits to water transport in *Juniperus osteosperma* and *Pinus edulis*: Implications for drought tolerance and regulation of transpiration, *Funct. Ecol.*, *12*, 906–911, doi:10.1046/j.1365-2435.1998.00275.x.

Mabuchi, K., Y. Sato, and H. Kida (2005), Climatic impact of vegetation change in the Asian tropical region. Part I. Case of the Northern Hemisphere summer, *J. Clim.*, *18*, 410–428, doi:10.1175/JCLI-3273.1.

Malhi, Y., and J. Grace (2000), Tropical forests and atmospheric carbon dioxide, *Trends Ecol. Evol.*, *15*, 332–337, doi:10.1016/S0169-5347(00)01906-6.

Malhi, Y., and J. Wright (2004), Spatial patterns and recent trends in the climate of tropical rainforest regions, *Philos. Trans. R. Soc. B*, *359*, 311–329, doi:10.1098/rstb.2003.1433.

Malhi, Y., L. E. O. C. Aragao, D. Galbraith, C. Huntingford, R. Fisher, P. Zelazowski, S. Sitch, C. McSweeney, and P. Meir (2009), Exploring the likelihood and mechanism of a climate-change-induced dieback of the Amazon rainforest, *Proc. Natl. Acad. Sci. U. S. A.*, *106*, 20,610–20,615, doi:10.1073/pnas.0804619106.

Manfroi, O. J., K. Kuraji, M. Suzuki, N. Tanaka, T. Kume, M. Nakagawa, T. Kumagai, and T. Nakashizuka (2006), Comparison of conventionally observed interception evaporation in a 100-m^2 subplot with that estimated in a 4-ha area of the same Bornean lowland tropical forest, *J. Hydrol.*, *329*, 329–349, doi:10.1016/j.jhydrol.2006.02.020.

Martínez-Vilalta, J., J. Piñol, and K. Beven (2002), A hydraulic model to predict drought-induced mortality in woody plants: An application to climate change in the Mediterranean, *Ecol. Modell.*, *155*, 127–147, doi:10.1016/S0304-3800(02)00025-X.

McDowell, N. G. (2011), Mechanisms linking drought, hydraulics, carbon metabolism, and vegetation mortality, *Plant Physiol.*, *155*, 1051–1059, doi:10.1104/pp.110.170704.

McDowell, N., et al. (2008), Mechanisms of plant survival and mortality during drought: Why do some plants survive while others succumb to drought?, *New Phytol.*, *178*, 719–739, doi:10.1111/j.1469-8137.2008.02436.x.

McNaughton, K. G., and P. G. Jarvis (1983), Predicting effects of vegetation changes on transpiration and evaporation, in *Water Deficits and Plant Growth*, vol. V, edited by T. T. Kozlowski, pp. 1–48, Academic, San Diego, Calif.

Meinzer, F. C., D. M. Johnson, B. Lachenbruch, K. A. McCulloh, and D. R. Woodruff (2009), Xylem hydraulic safety margins in woody plants: Coordination of stomatal control of xylem tension with hydraulic capacitance, *Funct. Ecol.*, *23*, 922–930, doi:10.1111/j.1365-2435.2009.01577.x.

Meir, P., P. M. Cox, and J. Grace (2006), The influence of terrestrial ecosystems on climate, *Trends Ecol. Evol.*, *21*, 254–260, doi:10.1016/j.tree.2006.03.005.

Melillo, J. M., A. D. McGuire, D. W. Kicklighter, B. Moore III, C. J. Vorosmarty, and A. L. Schloss (1993), Global climate change and terrestrial net primary production, *Nature*, *363*, 234–240, doi:10.1038/363234a0.

Metcalfe, D. B., et al. (2010a), Impacts of experimentally imposed drought on leaf respiration and morphology in an Amazon rain forest, *Funct. Ecol.*, *24*, 524–533, doi:10.1111/j.1365-2435.2009.01683.x.

Metcalfe, D. B., et al. (2010b), Shifts in plant respiration and carbon use efficiency at a large-scale drought experiment in the eastern Amazon, *New Phytol.*, *187*, 608–621, doi:10.1111/j.1469-8137.2010.03319.x.

Miralles, D. G., J. H. Gash, T. R. H. Holmes, R. A. M. de Jeu, and A. J. Dolman (2010), Global canopy interception from satellite observations, *J. Geophys. Res.*, *115*, D16122, doi:10.1029/2009JD013530.

Moorcroft, P. R., G. C. Hurtt, and S. W. Pacala (2001), A method for scaling vegetation dynamics: The ecosystem demography model (ED), *Ecol. Monogr.*, *71*, 557–586, doi:10.1890/0012-9615(2001)071[0557:AMFSVD]2.0.CO;2.

Myers, B. J. (1988), Water stress integral—A link between short-term stress and long-term growth, *Tree Physiol.*, *4*, 315–323.

Nakagawa, M., et al. (2000), Impact of severe drought associated with the 1997–1998 El Niño in a tropical forest in Sarawak, *J. Trop. Ecol.*, *16*, 355–367, doi:10.1017/S0266467400001450.

Nakicenovic, N., et al. (2000), *Special Report on Emissions Scenarios: A Special Report of Working Group III of the Intergovernmental Panel on Climate Change*, Cambridge Univ. Press, New York.

Neelin, J. D., C. Chou, and H. Su (2003), Tropical drought regions in global warming and El Niño teleconnections, *Geophys. Res. Lett.*, *30*(24), 2275, doi:10.1029/2003GL018625.

Nepstad, D. C., I. M. Tohver, D. Ray, M. Paulo, and G. Cardinot (2007), Mortality of large trees and lianas following experimental drought in an Amazon forest, *Ecology*, *88*, 2259–2269, doi:10.1890/06-1046.1.

Nobre, C. A., P. J. Sellers, and J. Shukla (1991), Amazonian deforestation and regional climate change, *J. Clim.*, *4*, 957–988, doi:10.1175/1520-0442(1991)004<0957:ADARCC>2.0.CO;2.

Phillips, O. L., et al. (2009), Drought sensitivity of the Amazon rainforest, *Science*, *323*, 1344–1347, doi:10.1126/science.1164033.

Phillips, O. L., et al. (2010), Drought-mortality relationships for tropical forests, *New Phytol.*, *187*, 631–646, doi:10.1111/j.1469-8137.2010.03359.x.

Porporato, A., F. Laio, L. Ridolfi, and I. Rodriguez-Iturbe (2001), Plants in water-controlled ecosystems: Active role in hydrologic processes and response to water stress. III. Vegetation water stress, *Adv. Water Resour.*, *24*, 725–744, doi:10.1016/S0309-1708(01)00006-9.

Porporato, A., E. Daly, and I. Rodriguez-Iturbe (2004), Soil water balance and ecosystem response to climate change, *Am. Nat.*, *164*, 625–632, doi:10.1086/424970.

Porporato, A., G. Vico, and P. A. Fay (2006), Superstatistics of hydroclimatic fluctuations and interannual ecosystem productivity, *Geophys. Res. Lett.*, *33*, L15402, doi:10.1029/2006GL026412.

Potts, M. D. (2003), Drought in a Bornean everwet rain forest, *J. Ecol.*, *91*, 467–474, doi:10.1046/j.1365-2745.2003.00779.x.

Priestley, C. H. B., and R. J. Taylor (1972), On the assessment of surface heat flux and evaporation using large-scale parameters, *Mon. Weather Rev.*, *100*, 81–92, doi:10.1175/1520-0493(1972)100<0081:OTAOSH>2.3.CO;2.

Rodríguez-Iturbe, I., and A. Porporato (2004), *Ecohydrology of Water-Controlled Ecosystems: Soil Moisture and Plant Dynamics*, Cambridge Univ. Press, New York.

Rodríguez-Iturbe, I., A. Porporato, L. Ridolfi, V. Isham, and D. R. Cox (1999), Probabilistic modelling of water balance at a point: The role of climate, soil and vegetation, *Proc. R. Soc. A*, *455*, 3789–3805, doi:10.1098/rspa.1999.0477.

Rodríguez-Iturbe, I., A. Porporato, F. Laio, and L. Ridolfi (2001), Intensive or extensive use of soil moisture: Plant strategies to cope with stochastic water availability, *Geophys. Res. Lett.*, *28*, 4495–4497, doi:10.1029/2001GL012905.

Sakai, S., R. D. Harrison, K. Momose, K. Kuraji, H. Nagamasu, T. Yasunari, L. Chong, and T. Nakashizuka (2006), Irregular droughts trigger mass flowering in aseasonal tropical forests in Asia, *Am. J. Bot.*, *93*, 1134–1139, doi:10.3732/ajb.93.8.1134.

Timmermann, A., J. Oberhuber, A. Bacher, M. Esch, M. Latif, and E. Roeckner (1999), Increased El Niño frequency in a climate model forced by future greenhouse warming, *Nature*, *398*, 694–697, doi:10.1038/19505.

van Nieuwstadt, M. G. L., and D. Sheil (2005), Drought, fire and tree survival in a Borneo rain forest, East Kalimantan, Indonesia, *J. Ecol.*, *93*, 191–201, doi:10.1111/j.1365-2745.2004.00954.x.

Werth, D., and R. Avissar (2005), The local and global effects of Southeast Asian deforestation, *Geophys. Res. Lett.*, *32*, L20702, doi:10.1029/2005GL022970.

West, A. G., K. R. Hultine, T. L. Jackson, and J. R. Ehleringer (2007), Contrasting hydraulic strategies explain differential summer moisture use of *Pinus edulis* and *Juniperus osteosperma*, *Tree Physiol.*, *27*, 1711–1720, doi:10.1093/treephys/27.12.1711.

World Resources Institute (2007), *EarthTrends: Environmental Information*, Washington, D. C. [Available at http://earthtrends.wri.org]

Yasunari, T. (1979), Cloudiness fluctuations associated with the Northern Hemisphere summer monsoon, *J. Meteorol. Soc. Jpn.*, *57*, 227–242.